# PARAMETRIC STUDY OF TWO DEGREE-OF-FREEDOM VORTEX-INDUCED VIBRATIONS OF A CYLINDER IN A TWO-DIMENSIONAL FLOW

**Didier LUCOR**[1] **and Michael S. TRIANTAFYLLOU**[2]

[1] *Institut Jean Le Rond d'Alembert, Unité Mixte CNRS-UPMC 7190, Université Pierre et Marie Curie, 4 place Jussieu, 75252 Paris Cedex 05, France.*

[2] *Department of Mechanical Engineering, 77 Massachusetts Avenue, Massachusetts Institute of Technology, Cambridge, MA 02139, USA.*

**Abstract.** We derive accurate, continuous response surfaces of two degree-of-freedom vortex-induced vibrations (VIV) of flexibly mounted cylinders, for a wide range of transverse and in-line natural frequencies, to identify the parametric sensitivity of the VIV response. The flow is assumed to be two-dimensional and the Reynolds number equal to 1,000; the structure has the same low damping for the in-line and transverse motions, while the transverse and in-line mass ratios are equal. The VIV response is studied within a wide range of the transverse natural frequency around the synchronization region. The variation of the in-line natural frequency is chosen to be larger than for the transverse natural frequency, in order to study multi-modal response. The numerical technique uses a stochastic generalized Polynomial Chaos representation coupled to a spectral element based deterministic solver; hence the response is obtained as a continuous function of the parameters.

**Key words:** two degree-of-freedom motion, VIV, surface response, sensitivity analysis.

## 1. Introduction

In vortex-induced vibration (VIV) studies of flexibly-mounted bluff bodies in cross-flow, often only the transverse motion of the body is considered, in order to simplify the problem. This is supported by the fact that the amplitude of vibrations along the in-line direction is generally much smaller than along the transverse direction, when the in-line and transverse natural frequencies are equal. Recently, it was reported that the effect of the in-line motion on the transverse motion can be significant when the natural frequency ratio $f_{n_X}/f_{n_Y}$ departs from one. The presence of the in-line $X$-motion can cause a significant change in the flow pattern behind the cylinder and may enhance the transverse $Y$-motion.

The purpose of the present study is to systematically explore the effects of the coupling of the two motions as function of the oscillator's natural frequencies. Instead of testing the response of the system for a finite set of values of the parameters, we use a method that provides us with a continuous representation of the response as a function of the variable parameters. We treat the natural frequencies of the oscillator as random quantities, in the sense that the frequencies are uncertain within specified ranges. This is often the case in complex operating environments when

the specific parameters of the system are known only approximately; hence, it is important to find the response as well as its sensitivity to parametric changes. The numerical technique we chose couples a stochastic generalized Polynomial Chaos (gPC) representation to a spectral element based deterministic solver. The power of the gPC representation resides in its ability to assign a given probability distribution to the parameters (the natural frequencies), and to propagate its effects through the model to the numerical solution (the VIV responses). The gPC model then provides fast and efficient approximations of the response for any set of natural frequencies within the study interval. The main advantage of the method from a numerical point of view is to significantly reduce the computational cost compared to, for example, the Monte-Carlo method.

## 2. Numerical method

We first introduce the general framework of the stochastic collocation method. Then we apply it to our fluid-structure interaction problem and briefly present the deterministic solver on which it relies.

### 2.1. Stochastic collocation method

The generalized Polynomial Chaos (gPC) method is a non-statistical method used to solve stochastic differential (SDE) and partial equations (SPDE) [21] and has been used for numerous applications [5, 6, 7, 15, 25]. It is a spectral representation of a random process in terms of orthogonal basis functions; the spatial and temporal evolutions of the basis coefficients provide quantitative estimates of the modeled random process solution. It is a means of representing second-order stochastic processes $X(\theta)$ parametrically through a set of independent random variables $\{\chi_j(\theta)\}_{j=1}^N, N \in \mathbb{N}$, through the events $\theta$ of a random event space $\Omega$. The approach is very similar to the variational finite elements formulation for deterministic mechanical problems [8]. The representation has the advantage of separating the stochastic variables (present only in the polynomial basis) from the deterministic ones (modal coefficients):

$$X(\theta) = \sum_{k=0}^{\infty} X_k \Phi_k(\boldsymbol{\chi}(\theta)). \tag{1}$$

Here $\{\Phi_j(\boldsymbol{\chi}(\theta))\}$ are orthogonal polynomials in terms of a zero-mean random vector $\boldsymbol{\chi} := \{\chi_j(\theta)\}_{j=1}^N$, satisfying the orthogonality relation $\langle \Phi_i \Phi_j \rangle = \langle \Phi_i^2 \rangle \delta_{ij}$.
For our application, we will only keep a finite set of random variables, i.e. $\{\chi_j\}_{j=1}^N$ with $N < 3$, and a $M$ finite-term truncation of (1). Due to its tensor-structure form, a complete basis has $M = (N+P)!/N!P!$ terms with $P$ being the highest polynomial order in the expansion. We will drop the $\theta$-dependence of $\boldsymbol{\chi}$ in the following for notation simplicity. We have:

$$X(\theta) = \sum_{k=0}^{M-1} X_k \Phi_k(\boldsymbol{\chi}). \tag{2}$$

The efficiency of the representation depends on the choice of the appropriate parametric family of random variables. There exists in (1) a one-to-one correspondence

between the type of the orthogonal polynomials $\{\Phi\}$ and the probabilistic law of the random variables $\boldsymbol{\chi}$. More details are given in [19, 26].
After solving for the deterministic coefficients $X_k$, we can obtain a response surface providing the sensitivity of the solution to the variability of the different parameters: The probability density function (pdf) of the solution can be evaluated, while, due to the orthogonality of the modes, the moments can be easily computed. The *mean* solution is contained in the expansion term with zero-index. The second moment, i.e., the *covariance* function is given by a linear combination of the modal fluctuations [8].
The stochastic collocation method [22] of the gPC is used herein. It does not require any substantial modifications to the existing deterministic solver, and consists of projecting the stochastic solution onto the orthogonal basis spanning the random space. The $X_k$ random coefficients can be directly computed as follows:

$$\forall k \ \in \{0, \ldots, M-1\} \quad X_k = \frac{< X(\boldsymbol{\chi}) \ \Phi_k(\boldsymbol{\chi}) >}{< \Phi_k^2(\boldsymbol{\chi}) >}. \tag{3}$$

The inner product is based on the measure $\rho(\boldsymbol{\chi})$ of the random variables:

$$\langle f(\boldsymbol{\chi}) g(\boldsymbol{\chi}) \rangle = \int_{\theta \in \Omega} f(\boldsymbol{\chi}) g(\boldsymbol{\chi}) d\mathcal{P}(\theta) = \int_{\Omega} f(\boldsymbol{\chi}) g(\boldsymbol{\chi}) \rho(\boldsymbol{\chi}) d\boldsymbol{\chi}, \tag{4}$$

with $\rho(\boldsymbol{\chi})$ denoting the density of the law $d\mathcal{P}(\theta)$ with respect to the Lebesgue measure $d\boldsymbol{\chi}$, and with integration taken over a suitable domain $\Omega$, determined by the range of $\boldsymbol{\chi}$. We recall that $< \Phi_k(\boldsymbol{\chi}) >= 0$ for $k > 0$ and the denominator $< \Phi_k^2(\boldsymbol{\chi}) >$ can be tabulated prior to the projection. The evaluation of (3) is equivalent to computing multi-dimensional integrals over the domain $\Omega$. Different ways of dealing with high-dimensional integrations can be considered, depending on the relative importance of accuracy versus efficiency [10]. A convenient approximation through numerical quadrature consists of replacing the integral by a finite weighted sum of the integrant values taken at selected points. When the number of grid points in multi-dimensions $N$ becomes too large, one should not use a grid based on the full tensor product of one-dimensional grids. An alternative is to use sparse quadratures [17, 16], which require less quadrature points. For instance, the sparse quadrature based on the Smolyak algorithm [20] has the advantage of remaining accurate with a convergence rate, which depends only weakly on the number of dimensions.
In this study, we used numerical quadratures of Gauss– and Gauss-Lobatto–type by full tensor products, because our number of random dimensions is small. We underline the fact that the deterministic solver will compute $X$ at those *known* quadrature points, not at randomly selected locations. The number of quadrature points $n_q$ depends on the regularity of the function to integrate. If it is well-known that $n_q$ points are enough to integrate *exactly* a polynomial function of leading order $P = (2 \times n_q - 1)$, but there is no way of knowing *a priori* how smooth the solution $X$ will be. The knowledge of the $\Phi_k$'s is not sufficient to foresee the regularity of the integrant. Therefore, we choose $n_q > P$ as our lower bound. The minimum number of sampling of the solution (or minimum number of calls to the deterministic solver) for the computation of the $k^{\text{th}}$ coefficient of (3), when the leading order of the $\Phi_k$ polynomial is $p$, is:

$$N_q = (n_q)^N \quad \text{with} \quad n_q = p + 1. \tag{5}$$

This number becomes $N_q = (P+1)^N$ for the estimation of the $M^{\text{th}}$ coefficient. Therefore, the minimum number of samplings to compute all $M$ coefficients $X_k$ is $(P+1)^N$.

### 2.2. Two degree-of-freedom structural model

The non-dimensional equations based on a reference length $D$ (cylinder diameter) and a reference velocity $U$ (inflow velocity), are:

$$\begin{aligned} \ddot{X} + 2\,\zeta_X\,\omega_X(\theta)\frac{\partial X}{\partial t} + \omega_X^2(\theta)X &= \frac{1}{2}\frac{C_{\text{Drag}}(t)}{m_X} \\ \ddot{Y} + 2\,\zeta_Y\,\omega_Y(\theta)\frac{\partial Y}{\partial t} + \omega_Y^2(\theta)Y &= \frac{1}{2}\frac{C_{\text{Lift}}(t)}{m_Y}, \end{aligned} \tag{6}$$

where $\omega_X(\theta) = 2\pi f_{n_X}(\theta)$ and $\omega_Y(\theta) = 2\pi f_{n_Y}(\theta)$ represent the natural frequencies of the oscillator in the $X$– and $Y$–directions, respectively. The $\theta$–dependency indicates that the natural frequencies are considered uncertain within a given interval. The forcing involves the non-dimensional time-dependent drag $C_{\text{Drag}}(t)$ and lift $C_{\text{Lift}}(t)$ coefficients, computed iteratively by the flow solver. The mass ratios of the structure are: $m_X = m_Y = m = \rho_s/\rho_f D^2 = 2$, ($\rho_s$ is the structural linear density and $\rho_f$ is the fluid density) and the damping ratios are: $\zeta_X = \zeta_Y = \zeta$ with $\zeta = 0$ or $\zeta = 3\%$ depending on the case under consideration. Dimensional frequency values $\hat{f}_n$ may be computed using a proper scaling: $\hat{f}_n = (f_n U)/D$. The reduced velocity is defined as $U_n = U/(\hat{f}_n D)$.

The hydrodynamic loads in (7) are computed using a two-dimensional Navier-Stokes direct numerical simulation (DNS) solver, the code $\mathcal{N}\varepsilon\kappa\mathcal{T}\alpha r$, based on the spectral/*hp* element method [9]. It was used previously for various VIV applications [13, 14, 12, 3]. A 2D rectangular grid of size $[(-22D; 55D) \times (-22D; 22D)]$ in the (x, y)–plane, and made of 708 triangular elements [11] with Jacobi polynomials of order $p = 11$, is used. This spatial resolution ensures the presence of (at least) 4 computational nodes within the flow boundary layer developing at the wall at $Re = 1,000$. Our chosen non-dimensional temporal resolution requires at least $10,000$ time iterations per period of oscillation. Time-statistics are collected over approximately 500 up to $1,000$ (when necessary) time units. In the following, we focus on the representation of natural frequencies using *uniform* distributions, so that only *bounded* variability ranges are considered, and no specific values are given preference within each interval; Legendre polynomials are chosen to represent the response. For stochastic processes that require more than one random dimensions to be represented, multi-dimensional Legendre polynomials are used, built in a tensor-like form.

Two generic cases are considered: In the first case (Case-A), we take $f_{n_X} = f_{n_Y} = f_n + \sigma\chi$, where $\chi$ has a uniform distribution with zero mean and unit variance. The parameters $f_n$ and $\sigma$ are constant, representing the mean value and half the width of variation of the natural frequency, respectively, chosen in such a way that $f_{n_X}$ and $f_{n_Y}$ are uniformly distributed in $[0.1114; 0.3024]$. Hence, only one uncertain parameter is considered, and $f_{n_X}/f_{n_Y} = 1$ always, while the damping factor is $\zeta = 0$; this serves as our reference case. In the second case (Case-B), we take $f_{n_X} = f_{n_1} + \sigma_1\chi_1$

and $f_{n_Y} = f_{n_2} + \sigma_2 \chi_2$, where $\chi_{1-2}$ are finite, independent, identically-distributed, uniform random variables with zero mean and unit variance. The parameters $f_{n_{1-2}}$ and $\sigma_{1-2}$ are constant and chosen such that $f_{n_X}$ and $f_{n_Y}$ are uniformly distributed in $[0.1273; 0.3820]$ and $[0.1273; 0.1910]$, respectively. The $f_{n_Y}$ range is narrower than in Case-A due to resolution requirements. This implies that the natural frequencies can vary independently and that $f_{n_X}/f_{n_Y} \in [0.5; 3]$. A damping factor of $\zeta = 3\%$ is used.
The output of the DNS simulations can be treated as a random field and decomposed onto the gPC basis (2). Herein, we focus mainly on the cylinder response statistics and show the drag force distribution; other physical quantities of interest can be evaluated similarly.
It is worth mentioning that gPC representations of complex and highly nonlinear processes are sometimes inefficient in capturing the correct behavior of the system; particularly for long-time integration of stochastic systems characterised by a limit cycle oscillation response. For these cases, it was found that a spectral decomposition of the solution in terms of global basis exhibits severe limitations [1, 24]. Herein, we circumvent this problem by considering the statistical moments of the simulated response and loads as functions of the uncertain parameters, instead of decomposing the time-dependent turbulent pressure and velocity fields.

## 3. Results

Continuous gPC representation of the cylinder response and loads are constructed using Legendre polynomials. To this end, the collocation procedure described in section 2.1 evaluates the deterministic solution of the VIV problem at certain discrete quadrature points in the parametric domain of interest. The deterministic DNS solver is therefore called for each *known* sample point, corresponding to a specific chosen pair of natural frequencies and time-statistics are collected for each case.

### 3.1. Case-A

Here, a multi-element gPC approach is employed along the lines introduced by Wan [23]. This allows to decompose the parametric domain into smaller subdomains and then use the gPC representation in each element. Local refinements in chosen elements are possible when local gradients are large and better accuracy becomes critical. Here, we use seven Gauss-Lobatto–quadrature points in each sub-element, and up to $P = 5^{\text{th}}$ order Legendre polynomials, to reconstruct the response.
Figure (1) presents the time traces of the cylinder displacement for different natural frequency pairs. Those signals are quite representative of the responses that can be encountered in our computations, both for Case-A and Case-B. In the first case, the motion eventually settles down to a regular, single pattern, after some initial transient time; this reflects on the cylinder trajectory as well. In the second case, the response alternates between regions with small and large amplitude, corresponding to multiple trajectory patterns. The frequency of occurrence of these regions is unpredictable and irregular. Those cases are the most difficult to simulate and require a long-time integration. Finally, the last signal is quite irregular at the small time-scale but exhibits some stationarity at the long time-scale. This diversity implies that the temporal statistics collected for each case will not bear the same

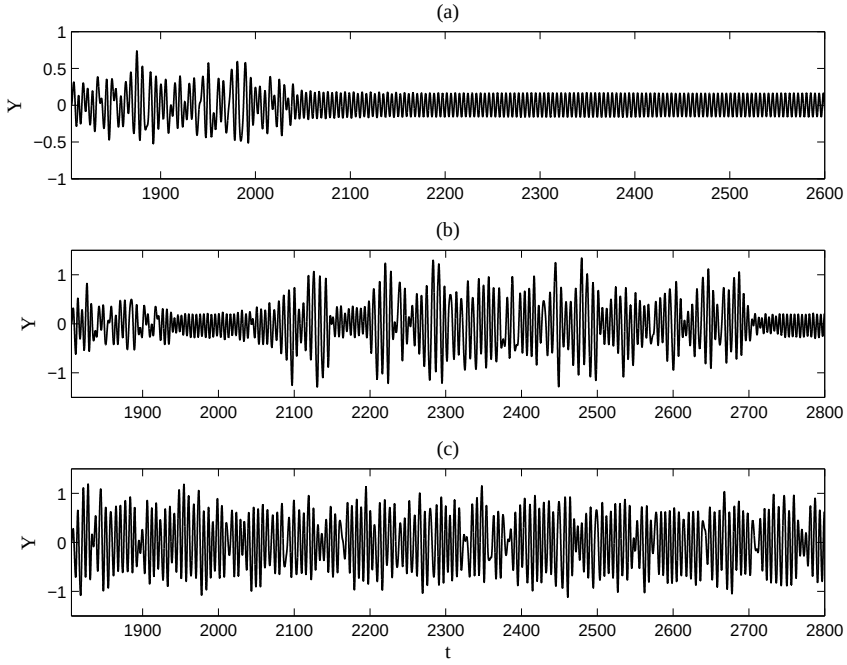


*Figure 1.* Time traces of the cylinder transverse $Y$-motion for different natural frequency pairs $(f_{n_X}, f_{n_Y})$.

level of regularity and confidence. In other words, the temporal statistics might not be fully converged. This will obviously affect the overall accuracy of some results of our study.

Figure (2) presents the gPC response of the average 10% highest amplitude of the $X$- and $Y$-motion against the reduced velocity; the symbols correspond to the DNS deterministic samplings. The dotted lines delimit the computational sub-elements used to obtain the response. The thin dashed curve with circles shows the one degree-of-freedom (transverse motion only) response of the same system and is used as reference. We emphasize that a maximum amplitude of $0.6D$ is what is usually reported in the literature and commonly accepted for 2D numerical simulations of one degree-of-freedom VIV [4]. We notice that allowing in-line motion enhances the maximum transverse cylinder motion relative to transverse-response only, with a 33% increase of the highest amplitude from around $0.6D$ to $0.8D$. Moreover, the maximum transverse amplitude of the two degree-of-freedom case does not coincide with the one of the one degree-of-freedom. We also notice that the gPC representation is more continuous and accurate for the $Y$- than for the $X$-motion, in particular for the $U_{n_Y} range \approx [5; 7]$. Interestingly, the distribution of the in-line amplitude closely follows the same peaks in the transverse amplitude.

### 3.2. Case-B

Figures (3) present the response surface of the average 10% highest amplitude of the $Y$-motion. This continuous surface is constructed with up to $P = 6^{\text{th}}$ order Legendre polynomials. The collocation procedure described in section 2.1 uses eight Gauss–quadrature points along each direction, which totals 64 DNS simulations. The deterministic solver is called for each quadrature point on the map, correspond-

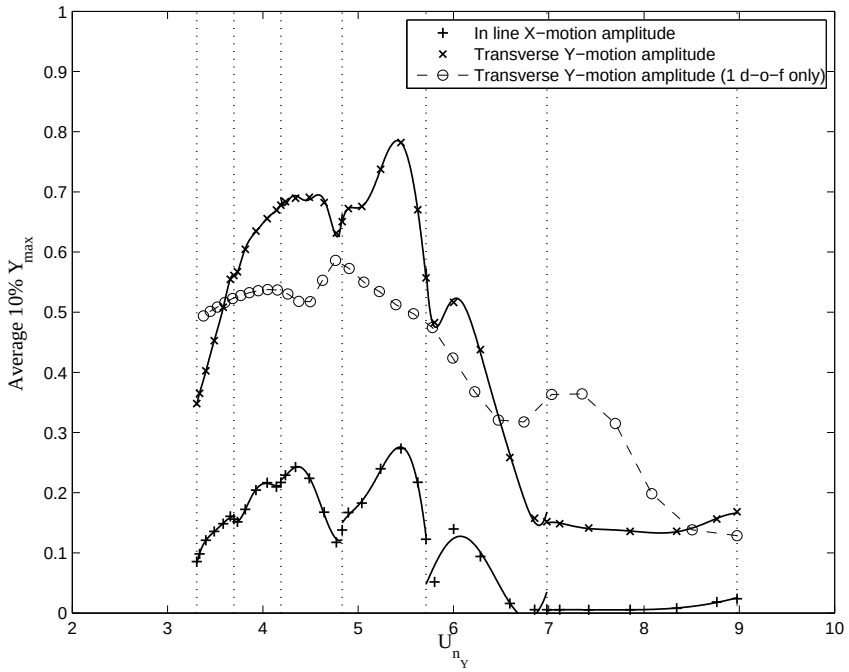


*Figure 2.* Average highest 10% $X$- and $Y$-motion amplitude responses vs. reduced velocity.

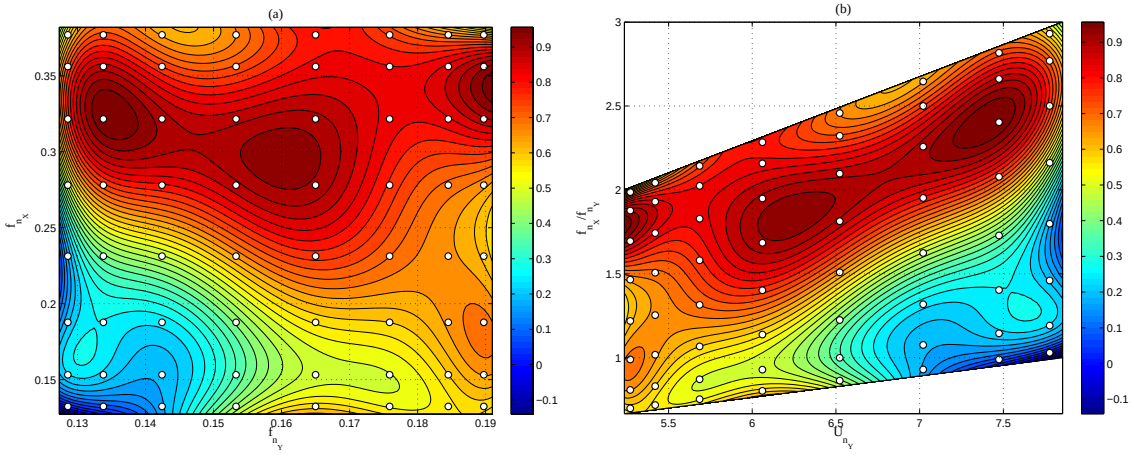


*Figure 3.* Average highest 10% $Y$-motion amplitude response. The white dots indicate the location of the sampling/quadrature points. (a): response surface vs. natural frequencies; (b): response surface vs. reduced velocity and frequency ratio.

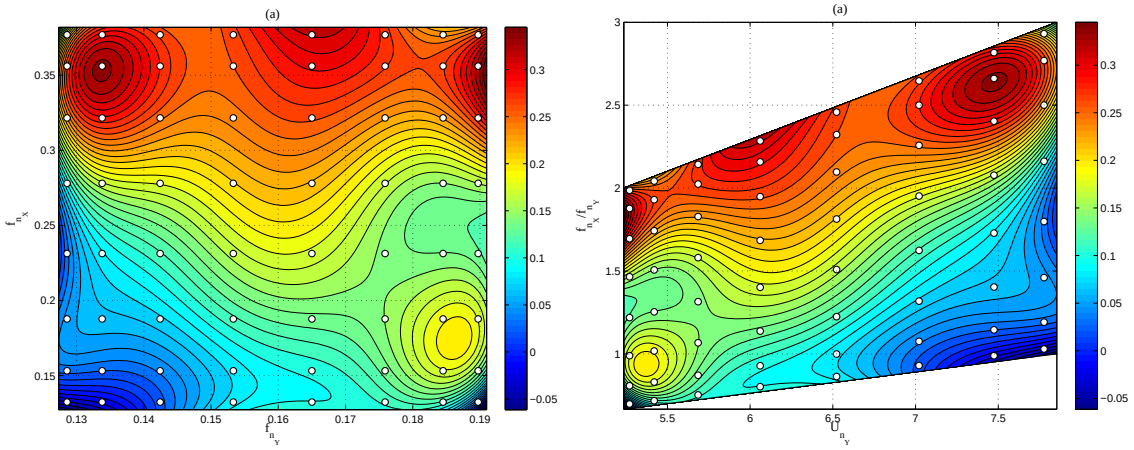


*Figure 4.* Average highest 10% $X$-motion amplitude response. The white dots indicate the location of the sampling/quadrature points. (a): response surface vs. natural frequencies; (b): response surface vs. reduced velocity and frequency ratio.

ing to a specific chosen set of parameters, represented by white dots in the figure. The negative values are due to end-effects and only affect very small regions of the domain. A measure of the error is obtained by comparing the exact DNS solution and the gPC reconstructed solution at the 64 sampling points. In this case, the $L_2$ norm of the error is within a 12% accuracy. The first finding is the increase of the transverse amplitude response compared to the case with no $X$-motion. Indeed, the maximum amplitude reaches up to 90% of the cylinder diameter $D$ for certain combinations of the natural frequencies. Nevertheless, this result is still below the experimental amplitude results when the flow is three-dimensional [2].

Figure (4-b) shows the same results presented differently, in the light of the experimental work of Dahl et al. [2]. The iso-contours are plotted vs. the reduced velocity (based on $f_{nY}$) and the natural frequency ratio $f_{nX}/f_{nY}$. Despite the somewhat reduced parametric ranges, it is clear that increasing the in-line to transverse frequency ratio causes a shift in the peak amplitude response to increasingly higher reduced velocities. This is in agreement with recent 3D-flow experimental results [2]. Moreover, we notice that at a frequency ratio between $[1.5; 2.0]$ two distinct response peaks appear; one centered around $U_{nY} \approx 5$ (and somewhat incomplete due to the range limitation), and one centered around $U_{nY} \approx 6.25$. This is in qualitative agreement with earlier experiments [18, 2]. Interestingly, there exists another peak centered around $U_{nY} \approx 7.35$ for higher in-line to transverse frequency ratios.

Figures (4) and (5) show the average 10% highest amplitudes of the $X$-motion and the drag coefficient distribution, respectively. The gPC representation of integrated quantities, such as the drag force on the cylinder, is very accurate, with the $L_2$ norm of the error exhibiting a 5% accuracy. As seen on the plots, there exists a strong relation between the drag forces and the $X$-motion; the mean drag force consistently increases for increasing frequency $f_{nX}$.

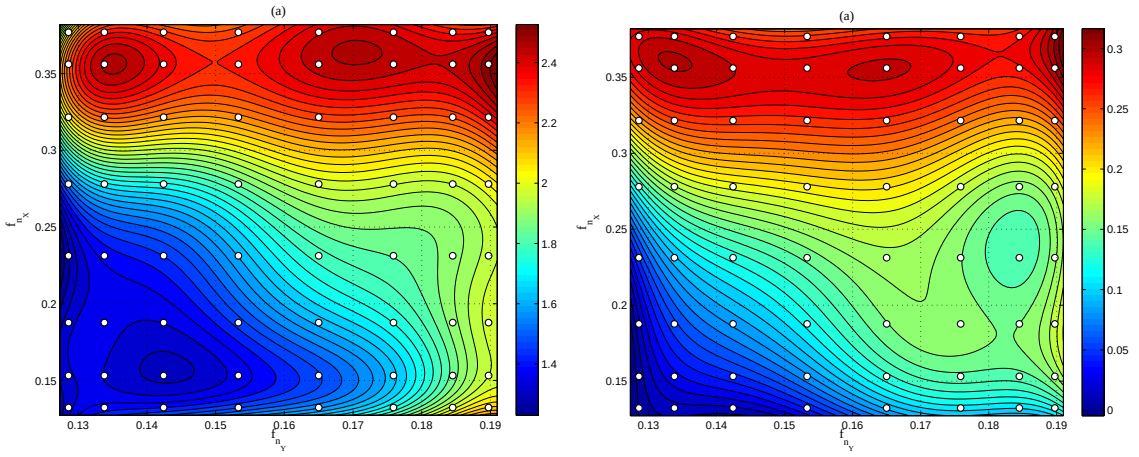


*Figure 5.* Drag coefficient response vs. natural frequencies. The white dots indicate the location of the sampling/quadrature points. (a): time-averaged drag coefficient $\overline{C_{\text{Drag}}}$; (b): *rms* drag coefficient $C_{\text{Drag}_{rms}}$.

## 4. Conclusions

This is a first application of recently developed numerical stochastic collocation techniques to obtain accurate, continuous response surfaces in two degree-of-freedom vortex-induced vibrations (VIV) of flexibly mounted cylinders; and to capture the sensitivity of the response to the change in both the transverse and in-line natural frequencies of the structure.

The system was studied for a wide range of transverse natural frequency around the synchronization region using a stochastic generalized Polynomial Chaos representation coupled to a DNS flow-structure interaction deterministic solver. Although the results are obtained assuming two-dimensional flow, the parametric dependence of the response is qualitatively close to observed results in experiments where the flow is three-dimensional: the in-line motion causes the maximum transverse response to increase by about 33%, but the peak responses occur at different reduced velocities and at multiple points. These results will guide us to explore a computationally more costly three-dimensional study of the same phenomenon.

## References

[1] P.S. Beran, C.L. Pettit, and D.R. Millman. Uncertainty quantification of limit-cycle oscillations. *Journal of Computational Physics*, 217(1):217–247, 2006.

[2] J. Dahl, F.S. Hover, and M.S. Triantafyllou. Two-degree-of-freedom vortex-induced vibrations using a force assisted apparatus. *Journal of Fluids and Structures*, 22:807–818, 2006.

[3] S. Dong and G.E. Karniadakis. DNS of flow past a stationary and oscillating cylinder at Re=10000. *Journal of Fluids and Structures*, 20:519–531, 2005.

[4] C. Evangelinos. *Parallel Simulations of VIV in Turbulent Flow: Linear and Non-Linear Models*. PhD thesis, Division of Applied Mathematics, Brown University, 1999.

[5] R. Ghanem and B. Hayek. Probabilistic modeling of flow over rough terrain. *J. Fluids Eng.*, 124(1):42–50, 2002.

[6] R.G. Ghanem. Ingredients for a general purpose stochastic finite element formulation. *Comp. Meth. Appl. Mech. Eng.*, 168:19–34, 1999.

[7] R.G. Ghanem and J. Red-Horse. Propagation of uncertainty in complex physical systems using a stochastic finite elements approach. *Physica D*, 133:137–144, 1999.

[8] R.G. Ghanem and P. Spanos. *Stochastic Finite Elements: a Spectral Approach*. Springer-Verlag, 1991.

[9] G.E. Karniadakis and S.J. Sherwin. *Spectral/hp Element Methods for CFD*. Oxford University Press, 1999.

[10] Andreas Keese. *Numerical solution of systems with stochastic uncertainties: a general purpose framework for stochastic finite elements*. PhD thesis, Technische Universitat Braunschweig, Mechanik-Zentrum, 2005.

[11] D. Lucor. *Generalized Polynomial Chaos: Applications to Random Oscillators and Flow-Structure Interactions*. PhD thesis, Brown University, 2004.

[12] D. Lucor, J. Foo, and G.E. Karniadakis. Vortex mode selection of a rigid cylinder subject to VIV at low mass-damping. *Journal of Fluids and Structures*, 20:483–503, 2005.

[13] D. Lucor, L. Imas, and G.E. Karniadakis. Vortex dislocations and force distribution of long flexible cylinders subjected to sheared flows. *Journal of Fluids and Structures*, 15:641–650, 2001.

[14] D. Lucor and G.E. Karniadakis. Effects of oblique inflow in vortex induced vibrations. volume 71, pages 375–389, 2003.

[15] D. Lucor and G.E. Karniadakis. Noisy Inflows Cause a Shedding-Mode Switching in Flow past an Oscillating Cylinder. *Physics Review Letters*, 92(15):154501–1; 154501–4, 2004.

[16] Erich Novak and Klaus Ritter. High dimensional integration of smooth functions over cubes. *Numerische Mathematik*, 75:79–97, 1996.

[17] Erich Novak and Klaus Ritter. Simple cubature formulas with high polynomial exactness. *Constructive Approximation*, 15:499–522, 1999.

[18] T. Sarpkaya. Hydrodynamic damping, flow-induced oscillations, and biharmonic response. *ASME Journal of Offshore Mechanics and Arctic Engineering*, 117:232–238, 1995.

[19] W. Schoutens. *Stochastic Processes and orthogonal polynomials*. Springer-Verlag, New York, 2000.

[20] S.A. Smolyak. Quadrature and interpolation formulas for tensor products of certain classes of functions. *Soviet. Math. Dokl.*, 4:240–243, 1963.

[21] P. Spanos and R.G. Ghanem. Stochastic finite element expansion for random media. *ASCE J. Eng. Mech.*, 115(5):1035–1053, 1989.

[22] M. Tatang, W. Pan, R. Prinn, and G. McRae. An efficient method for parametric uncertainty analysis of numerical geophysical models. *Journal of Geophysical Research*, 102:21925–21932, 1997.

[23] X. Wan and G.E. Karniadakis. An adaptive multi-element generalized polynomial chaos method for stochastic differential equations. *Journal of Computational Physics*, 209:617–642, 2005.

[24] X. Wan and G.E. Karniadakis. Long-term behavior of polynomial chaos in stochastic flow simulations. *Comput. Methods Appl. Mech. Engrg.*, 195:5582–5596, 2006.

[25] X. Wan and G.E. Karniadakis. Stochastic heat transfer enhancement in a grooved channel. *Journal of Fluid Mechanics*, 565:255–278, 2006.

[26] D. Xiu and G.E. Karniadakis. The Wiener-Askey polynomial chaos for stochastic differential equations. *SIAM J. Sci. Comput.*, 24(2):619–644, 2002.